Background Shape Study of the Invariant Higgs Mass Spectrum of the $t\bar{t}H^0$ Channel

1st Year Report

Catrin Bernius

Supervisor:
Dr. Nikos Konstantinidis

Department of Physics and Astronomy
University College London

June 11, 2007

Abstract:

One of the most promising channels in which a low mass Higgs search could be successful is the $t\bar{t}H^0$ associated production where the Higgs boson decays into a pair of b quarks. The reconstruction of two top quarks in the final state allows the background to be suppressed. Nevertheless, in order to be able to estimate the signal contribution the background contribution to the $t\bar{t}H^0$ $H^0 \rightarrow b\bar{b}$ channel has to be understood, especially the contribution of the irreducible $t\bar{t}b\bar{b}$ (QCD) background.
This report investigates two different techniques of distinguishing signal events from background events based on the shape of the signal and $t\bar{t}b\bar{b}$ background in the invariant mass spectrum of the reconstructed Higgs candidates. These techniques are developed with respect to their application in data. The study is based on a fast simulation of the ATLAS detector, which is currently under construction at the future proton-proton collider LHC.

Contents

1 Theory

This chapter briefly explains how the Higgs mechanism comes is included in the Standard Model and also gives information about the production and decay of the Higgs boson in the $t\bar{t}H^0$ channel. The background contributions to this channel are also discussed.

1.1 The Standard Model and the Higgs boson

The fundamental components of matter and their interactions are described by a very successful theory, the Standard Model. This Model is based on renormalizable quantum gauge field theory. A system of particles is described by a Lagrangian, a function that summarizes the dynamics of a system. The invariance of a Lagrangian under continuous symmetry operations is the source of conserved quantities. Local gauge symmetries are local transformations of a particle wave function which leave the Lagrangian unchanged. The interaction between particles via gauge bosons is described by such a local symmetry, the symmetry itself forms a symmetry group and is related to a particular force. So the electromagnetic force is related to the group U(1), the weak force to SU(2) and the strong force to SU(3).

The gauge theory of the electroweak interactions implies that all gauge bosons must be massless. But experimental results disagree with this since only the photon is massless whereas the other gauge bosons Z^0, $W^{\pm}$ and W have been observed to be massive. Nevertheless explicit mass terms like $\frac{M^2}{2}W_\mu W^\mu$ in the electroweak Lagrangian destroy the local gauge invariance and make the theory meaningless.

This is where the Higgs Mechanism comes in. The fundamental idea is to introduce an extra field in the theory which is non-zero in the ground state. The generation of mass then takes place by interactions of fermions and gauge bosons with this field [1]. This is possible when the spontaneous symmetry breaking occurs. The Higgs boson H^0 is a consequence of this mechanism.

It is one of the main objectives of the Large Hadron Collider (LHC) to discover the Higgs boson. The following sections describe the production and decay of the Higgs boson at the LHC.

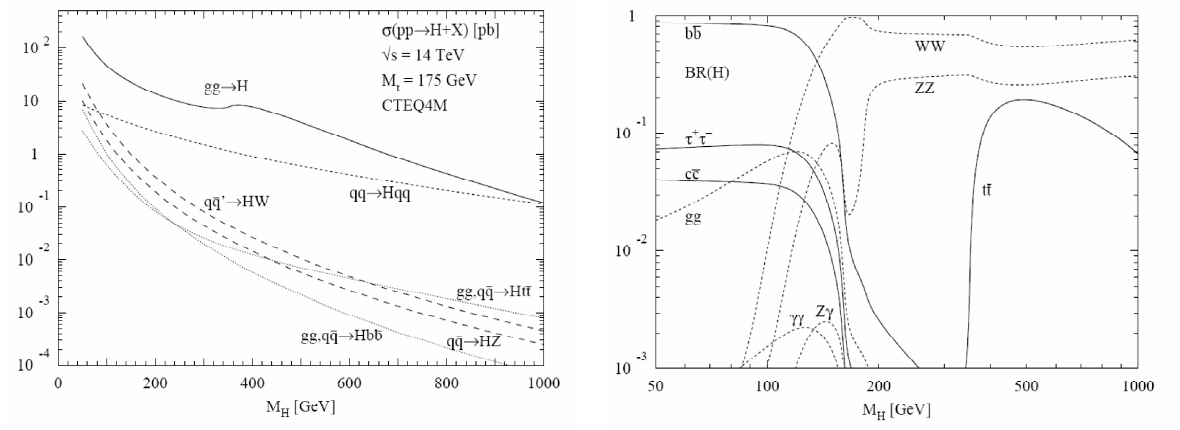

Figure 1.1: Left: Higgs production cross-section as a function of Higgs mass [2]. Right: Branching ratios of the dominant decay modes of the SM Higgs particle [2].

1.2 Higgs production and decay at the LHC

Several Higgs production methods at the LHC can lead to observable cross-sections depending on the mass of the Higgs boson. These include gluon-gluon fusion, WW and ZZ fusion and associated production with W and Z boson as well as with $t\bar{t}$. The Higgs production cross section as a function of the Higgs mass is shown in the left plot in Figure 1.1.

The Higgs boson decay depends strongly on its mass since it couples preferentially to heavy particles and therefore decays primarily into the highest mass particles energetically allowed. Figure 1.1 (right) shows the branching ratios of the dominant decay modes of the Higgs boson as a function of the Higgs mass.

The mass region of interest is the low mass region from $110\text{GeV} < m_{H^0} < 130\text{GeV}$. In this mass region the dominant decay mode is $H^0 \to b\bar{b}$ with a branching ratio up to 85%. Nevertheless the signal extraction of the direct Higgs production $gg \to H^0 \to b\bar{b}$ will be very difficult due to the large QCD background and the need to trigger on the dijet final state since there is no such trigger.
A trigger is therefore needed, e.g. isolated leptons. They are provided by processes containing $W^{\pm}$ or Z^0 and $t\bar{t}H^0$ production. But channels with $W^{\pm}$ or Z^0 suffer from large $W^{\pm}$ + jets and Z^0 + jets backgrounds [3]. The $t\bar{t}H^0$ production in the final state $l\nu b\,jjb\,b\bar{b}$ in contrast is more promising. Despite the smaller cross section, tagging of four b-jets helps to reduce backgrounds from $t\bar{t}$ + jets, $W^{\pm}$ + jets and Z^0 + jets.

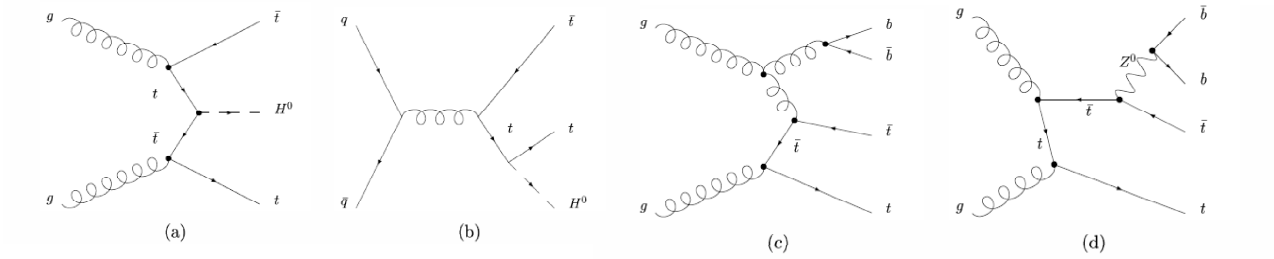

Figure 1.2: Example Feynman diagrams for the processes (a) $gg \to t\bar{t}H^0$, (b) $q\bar{q} \to t\bar{t}H^0$, (c) $gg \to t\bar{t}b\bar{b}$ and (d) $gg \to Z/W/\gamma^* \to t\bar{t}b\bar{b}$.

1.3 Study of the channel $t\bar{t}H^0$, $H^0 \to b\bar{b}$ and its background contributions

At the LHC, the $t\bar{t}H^0$ state is produced via gluon-gluon interaction in about 90% and in quark-quark interation in 10% of all cases. Typical Feynman diagrams are shown in Figure 1.2 (a, b). Top quarks decay almost exclusively into Wb, and W bosons decay hadronically in about 2/3 of all cases, and into electron/muon plus electron-/muon-neutrino in about 1/3 of all cases. The $t\bar{t}$ final state with the highest branching fraction is jjb jjb. Including $H^0 \to b\bar{b}$ this would result in a purely hadronic multi-jet final state with moderate transverse momentum of the jets for which no trigger is foreseen in the ATLAS experiment. In order to get a handle for triggering $t\bar{t}H^0$ events, one requires one top quark to decay semileptonically, leading to a final state of $\ell\nu$bjjbbb with 4 b-jets, 2 light jets, 1 lepton (only electrons and muons are considered) and missing transverse momentum.

The main background to the signal process arises from QCD processes with a top-quark pair and additional jets from initial and final state gluon radiation. The cross section for the $t\bar{t}$ + jets background is about 900 times larger than that of the signal. But the additional jets are heavily dominated by light flavours and can be suppressed by requiring four b-jets, so only a small fraction consists of true $t\bar{t}b\bar{b}$ events. Some differentiation between b-jets and jets from lighter quark flavours is possible by exploiting life-time and decay information of the original quarks. Hadrons containing b-quarks have a substantially larger lifetime than hadrons without b-quarks, so that at LHC energies b-hadrons travel a few millimeters before decaying.
A less severe $t\bar{t}b\bar{b}$ background is mediated by electroweak gauge bosons, $gg \to Z/\gamma * /W \to t\bar{t}b\bar{b}$. The cross section for these processes is nine times smaller than $t\bar{t}b\bar{b}$ production from QCD. Typical Feynman diagrams for those processes are shown in 1.2 (c) and (d).
Other backgrounds are negligible as long as four tagged b-jets are required.

2 The LHC and the ATLAS Experiment

The Large Hadron Collider (LHC) [4] is a proton-proton collider, currently being constructed at CERN. It is contained in a 27 km circumference tunnel located underground which was formerly used to house the electron-positron collider LEP. The LHC will accelerate two beams of protons in opposite directions up to a beam energy of 7 TeV which results in a center of mass energy of 14 TeV. The beams, each containing about 3×10^{14} protons are brought to collisions at four interaction points. The design luminosity is 10^{34} $\mathrm{cm}^{-2}\mathrm{s}^{-1}$.

The ATLAS (A Toroidal LHC ApparatuS) detector [3, 5] is one of the four detectors at the LHC. ATLAS is designed as an omni purpose detector to fully exploit the discovery potential of the LHC. The detector has a cylindrical symmetry with a diameter of 22 m, a length of 42 m, and a weight of almost 7000 tons.

The parameters of the LHC and the challenging physics program put high demands on the components of ATLAS: A powerful tracking system is needed which can resolve even low transverse momentum tracks in the dense environment expected at design luminosity, hermetic calorimeters with a very good energy resolution for electrons and photons and a reliable measurement of the missing transverse energy, and a precise spectrometer for measuring the momenta of muons. The ATLAS detector has a large acceptance in pseudorapidity. An overview picture of the ATLAS detectors is shown in Fig. 2.1. The three main components of the detector are the Inner Detector, the Calorimeter (Electromagnetic and Hadronic) and the Muon Spectrometer.

The geometry of the ATLAS detector is descriped by using the transverse momentum $\mathrm{p_T}$ pseudorapidity $\eta$and the azimuth angle ϕ. The pseudorapidity is related to the angle θ between a particle and the z-axis by $\eta = -\ln(\tan(\theta/2))$.

The Inner Detector consists of three distinct sub-systems which are all contained in a solenoid magnetic field of 2T. Near the interaction point there is a high resolution Pixel detector and a Semi-Conductor Tracker (SCT). These use silicon microstrip and pixel technologies respectively to satisfy the momentum and vertex resolution requirements for high-precision measurements at the expected very large track density at the LHC. Radially outermost is the Transition Radiation Tracker (TRT) which is designed to give an extendend lever-arm for improved transverse momentum $\mathrm{p_T}$ measurement. The magnet surrounding the entire inner detector causes charged particles to curve in the xy plane, the direction of the curve reveals a particle's charge and the degree of curvature reveals its transverse momentum. The performance of the Inner Detector is

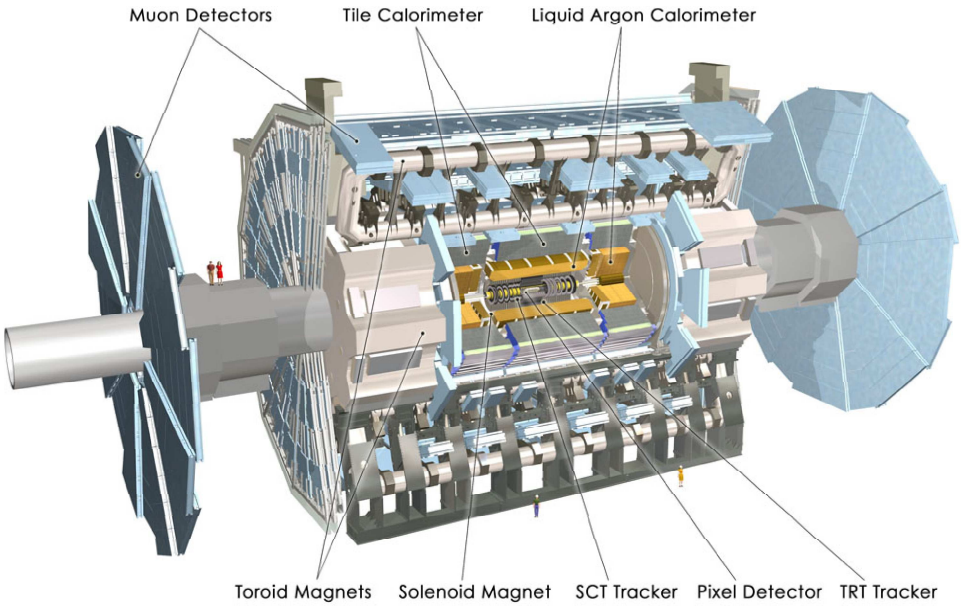

Figure 2.1: The built-up of the ATLAS detector.

important for the $t\bar{t}H^0$ channel because tracks provide lifetime information expected from jets with b-quarks.

The electromagnetic calorimeter is a high granularity sampling calorimeter, assembled from alternating layers of lead, to develop the shower, and liquid argon (LAr) as active material to detect the particles produced. The hadronic calorimeter uses scintillators with Fe and Cu Tiles as absorbers to measure the energy of jets and hadronic particles.

The Muon spectrometer is an outstanding feature of the ATLAS detector. Its design is based on magnetic deflection of muons in a system of three large superconducting toroid magnets. It serves as trigger for many signatures and provides measurement of muon momenta independent from the Inner Detector.

The bunch crossing rate at LHC is one every 25 ns (40 MHz), giving on average 23 proton-proton interactions per bunch crossing at design luminosity. Due to computing power and storage capability restrictions, the rate of recorded events has to be reduced to approximately 100 Hz. This has to be done by a unbiased selection strategy which has to ensure that rare signals will not be missed whilst proving an efficient rejection of high rate backgrounds. The ATLAS trigger and data acquisition system [6] is based on three levels of online event selection, each trigger level refines the decisions made at the previous level and applies additional selection criteria.

3 Study of the $t\bar{t}b\bar{b}$ Background of the Channel $t\bar{t}H^0, H^0 \rightarrow b\bar{b}$

In order to be able to select signal events, it is crucially important to understand the contribution of background events. The $t\bar{t}b\bar{b}$ background is an irreducible dominant background to the $t\bar{t}H^0$ channel, since it has the same final states as the $t\bar{t}H^0$ channel, therefore it is very important to understand the background shape of the invariant mass distribution of the Higgs candidate. This chapter describes the work towards fitting the background shape. First the cut based analysis used to select possible signal events is described. Then a comparison of the decay topology and the effect on kinematic variables of the $t\bar{t}b\bar{b}$ and $t\bar{t}H^0$ channel is done in order to enhance the understanding of differences between the two channels. Finally the work done towards fitting the $t\bar{t}b\bar{b}$ shape is described.

3.1 Cut based analysis

The analysis used to select candidate events is a cut based analysis which consists of five event reconstruction steps.
The first step is the selection of events with a topology which is compatible with that of the signal. Therefore an isolated lepton (either an electron or a muon) with $p_T^e > 20\text{GeV}$ or $p_T^\mu > 6\text{GeV}$ within the η region of the inner detector of $|\eta| < 2.5$ is required. Additionally four jets, which pass the b-tagging cut, are tagged as b-jets and two non-b tagged jets with $p_T > 20\text{GeV}$ and $|\eta| < 5$ (the extent of the calorimeter system in η) are also required.
The second step is the reconstruction of the leptonic W, which is limited by the incomplete reconstruction of the neutrino four-momentum. Due to an incomplete coverage of the detector around the beam pipe, p_z^ν can not be estimated from the missing momentum in the event. It is possible to recover some information about p_z^ν by solving the equation for the W boson mass in terms of the two constituents (with $p_x^\nu = p_x^{miss}, p_y^\nu = p_y^{miss}$ and assuming the neutrino is massless):

$$m_W^2 = (E^\nu + E^l)^2 - (p_x^\nu + p_x^l)^2 - (p_y^\nu + p_y^l)^2 - (p_z^\nu + p_z^l)^2 \tag{3.1}$$

For events where equation 3.1 cannot be solved due to a negative square-root term in the quadratic solution, the reconstruction is done by a collinear approximation where $p_z^\nu = p_z^l$.

	$\epsilon(t\bar{t}H^0)$	$\epsilon(t\bar{t}b\bar{b})$
Jet Preselection	9.08%(9.08%overall)	3.43%(3.43%overall)
Lepton Preselection	66.33%(6.02%overall)	66.85%2.29%overall)
Leptonic W reconstruction	89.42%(5.39%overall)	90.06%(2.07%overall)
Hadronic W reconstruction	75.43%(4.06%overall)	76.91%(1.59%overall)
$t\bar{t}$ reconstruction	55.88%(2.27%overall)	50.66%(0.80%overall)
Higgs boson reconstruction	35.30%(0.80%overall)	25.72%(0.20%overall)

Table 3.1: Selection efficiencies for the $t\bar{t}H^0$ signal and $t\bar{t}b\bar{b}$ background sample after the Lepton and Jet Preselection, the leptonic and hadronic W reconstruction, the $t\bar{t}$ and finally the Higgs boson reconstruction.

Thirdly, hadronic W candidates are created from pairs of non-b-tagged jets. Those pairs with an invariant mass $m_{jj} = m_W \pm 25\text{GeV}$ are kept, where m_W the nominal W boson mass is.
Both top-quarks are reconstructed simultaneously finding the combination of b-jets and W candidates that minimises equation 3.2. This is the fourth step of the reconstruction.

$$\Delta^2 = (m_{l\nu b} - m_t)^2 + (m_{jjb} - m_t)^2 \tag{3.2}$$

A cut is then applied to keep events where both reconstructed top masses lie within ±20GeV of the nominal top mass.
Finally, the remaining b-jets are assigned to the Higgs boson decay. If more than two b-jets remain, then the two with the highest p_T are chosen. Events within a ±30GeV window of the nominal Higgs boson mass are retained at the end of the analysis.

The following sections, will refer to this selection as the *standard selection*. Table 3.1 summarizes the selection efficiencies for the $t\bar{t}H^0$ signal and $t\bar{t}b\bar{b}$ (QCD) background (full simulation) for each of the five reconstruction steps in full simulation with the current analysis.

3.2 Characteristics of signal and background processes

In this section, only the signal and main background, $t\bar{t}b\bar{b}$ via the QCD interaction are considered.
In order to enhance the understanding of properties of the $t\bar{t}H^0$ and $t\bar{t}b\bar{b}$ background, a comparison of some kinematic variables is done. The histograms shown in this section were obtained using full simulation (see Appendix A) of the $t\bar{t}H^0$ and $t\bar{t}b\bar{b}$ samples of the cut based analysis.

Figure 3.1 and 3.2 show the p_T and η distribution for light and b-jets in signal and $t\bar{t}b\bar{b}$ background events. The $t\bar{t}b\bar{b}$ background has a softer p_T spectrum for b-jets than the $t\bar{t}H^0$ sample, whereas for light jets, there is no significant difference noticeable. One could possibly expect an even softer p_T spectrum for b-jets in the $t\bar{t}b\bar{b}$ sample, but the gluon is a spin 1 particle,

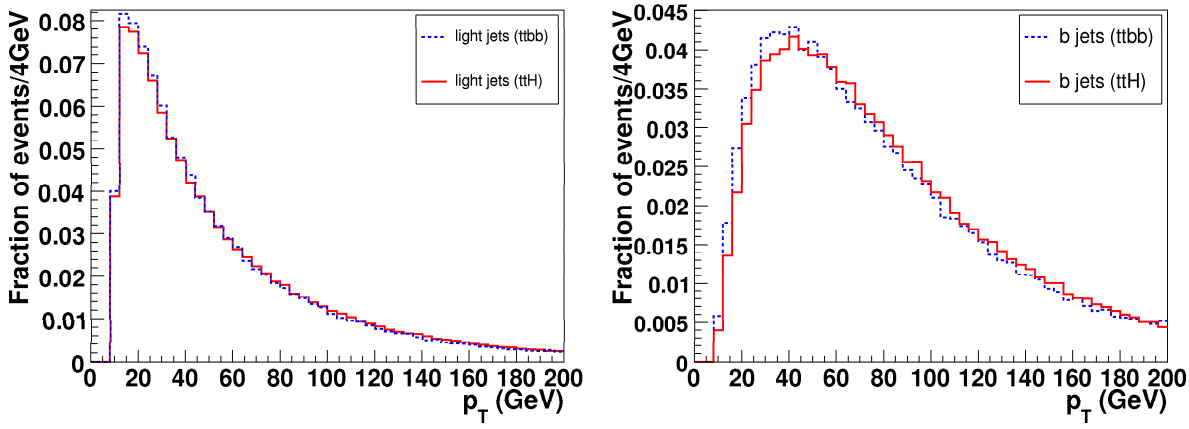

Figure 3.1: p_T distribution for light (left) and b-jets (right) in signal and $t\bar{t}b\bar{b}$ background events. Histograms are normalised to unit area.

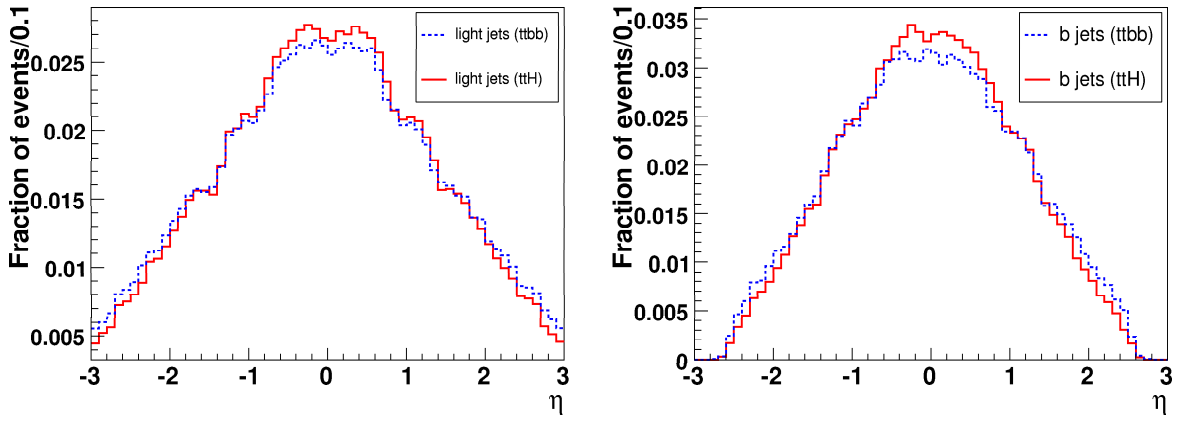

Figure 3.2: η distribution for light (left) and b-jets (right) in signal and $t\bar{t}b\bar{b}$ background events. Histograms are normalised to unit area.

which implies that the two spin-1/2 decay products prefer to align along the original gluon momentum direction. Therefore it is more likely that these decay products are reconstructed in one b-jet. This will then make the p_T distribution harder. It is not likely that this happens for the decay products of the Higgs boson, since this is a spin 0 particle and therefore there is no directional preference for the decay products due to spin.
Light jets as well as b-jets tend to be more central in η in the $t\bar{t}H^0$ sample whereas the η distribution for $t\bar{t}b\bar{b}$ events has larger contributions in the forward region.

In Figure 3.3 the multiplicities of b-jets (right) and light jets (left) of the $t\bar{t}H^0$ and $t\bar{t}b\bar{b}$ sample

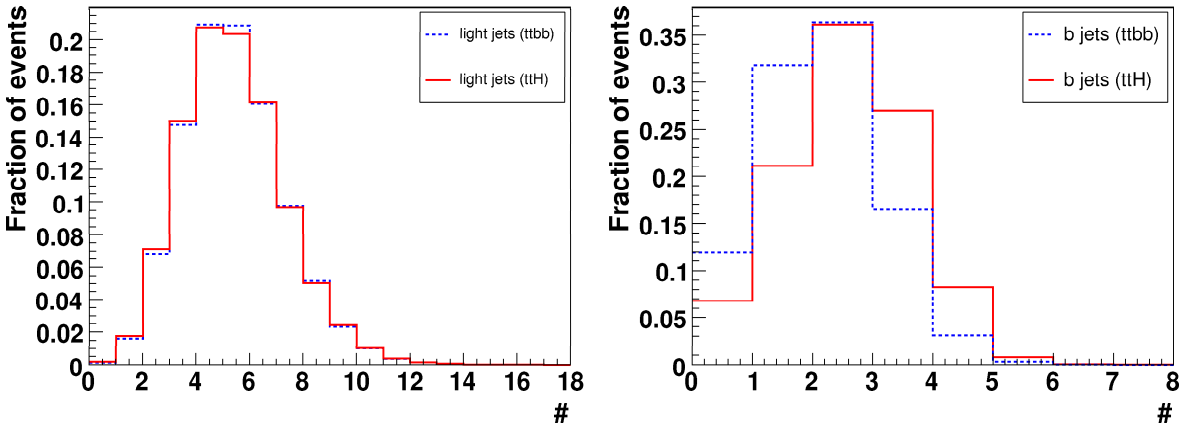

Figure 3.3: Light-jet (left) and b-jet (right) multiplicities for signal and QCD $t\bar{t}b\bar{b}$ background. Histograms are normalised to unit area.

are shown. Light jets tend to have a very similar distribution in signal and background with an average number of 4.9 jets in a signal event compared to also 4.9 jets of the $t\bar{t}b\bar{b}$ sample. For b-jets, the average number is 1.1 in signal and 1.7 in $t\bar{t}b\bar{b}$ events. The reconstruction of $t\bar{t}H^0$ events requires at least 4 b-jets. In this region the $t\bar{t}b\bar{b}$ sample has a lower multiplicity and therefore the efficiency of passing this requirement is about 3 times higher for $t\bar{t}H^0$ events than for $t\bar{t}b\bar{b}$ events (see jet preselection efficiency in table 3.1).

A jet is tagged as a b-jet when the jet weight is greater than 3. The calculation of a weight for a jet is based on the impact parameter, the distance to the closest approach to the primary vertex (see Appendix B). The weight distribution for all jets (light and b-jets) is shown in Figure 3.4 over the full range (left) and zoomed in the range which is relevant for b-tagging (right). The $t\bar{t}H^0$ sample has a slightly higher distribution in the for the b-tagging relevant area than the $t\bar{t}b\bar{b}$ sample. By applying a cut on a particular value, more jets from $t\bar{t}H^0$ than $t\bar{t}b\bar{b}$ events are accepted which results in a higher multiplicity of b-jets for the $t\bar{t}H^0$ sample.

3.3 Study of the $t\bar{t}b\bar{b}$ background shape

For an estimation and extraction of the $t\bar{t}H^0$ signal peak in the m_{bb} mass spectrum it is important to know and understand the shape of the background, especially the main contribution of the irreducible $t\bar{t}b\bar{b}$ background from QCD. In this section, only the signal and $t\bar{t}b\bar{b}$ background events from QCD are considered.
This section starts with the development of a selection which produces a more significant difference between the shapes of the reconstructed m_{bb} spectrum in signal and background. This

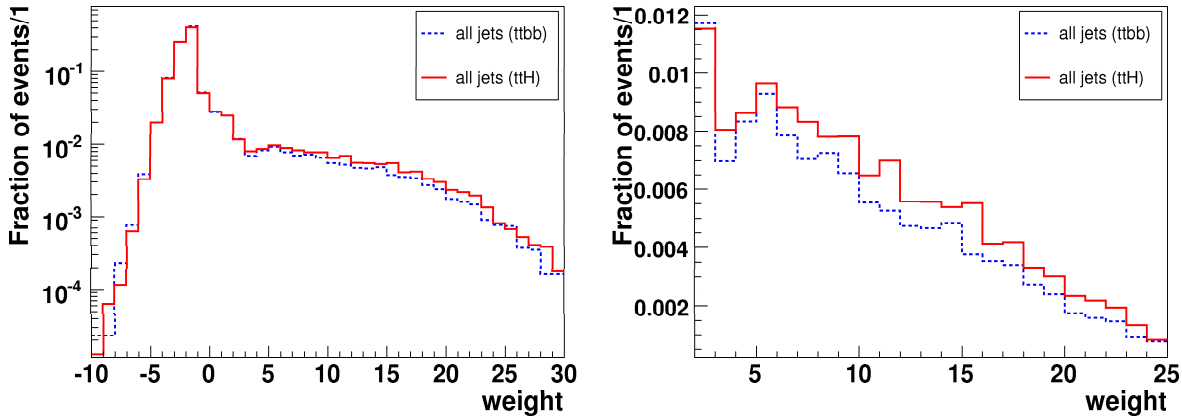

Figure 3.4: Jet weight distribution for all jets over the full range (left) (normalized to unit area) and zoomed in the b-tagging relevant range (right).

provides some insight into how the background shape varies with different inputs. To further develop the understanding and to find a function which describes the background shape, a fit is applied. This is followed by a discussion of possible approaches for signal estimation.
The aim of this background study is to consider and develop several possible techniques for signal estimation. With the Monte Carlo simulated events it is possible to get an idea of how the background and also the signal distribution could be described with a fit function. These should provide a starting point for a fit-based analysis in real data when the LHC begins operating. The procedure then would be to select a predominantly $t\bar{t}b\bar{b}$ sample by e.g. inverting cuts of the analysis. This distribution is then fitted and the estimation techniques described below can then be applied to the selected candidate $t\bar{t}H^0$ sample. It would then be possible to evaluate the statistical likelihoods that the candidate sample contains purely background and that it contains something else in addition to the expected background. The more likely scenario could then be established. This can be achieved using different goodness of fit techniques, like the χ^2 method or the Kolmogorov-Smirnov test.
For this study 1 million $t\bar{t}b\bar{b}$ events have been generated with the AcerMC Monte-Carlo event generator . For signal events, 38950 $t\bar{t}H^0$ events were used.

3.3.1 Tight selection

Several kinematic cuts of the standard selection were varied in order to change the background shape in a more distinguishable way from the signal shape. This was done starting each time from the standard selection, changing one cut at a time.

A cut variation on the transverse energy E_T of electrons and muons was applied and the re-

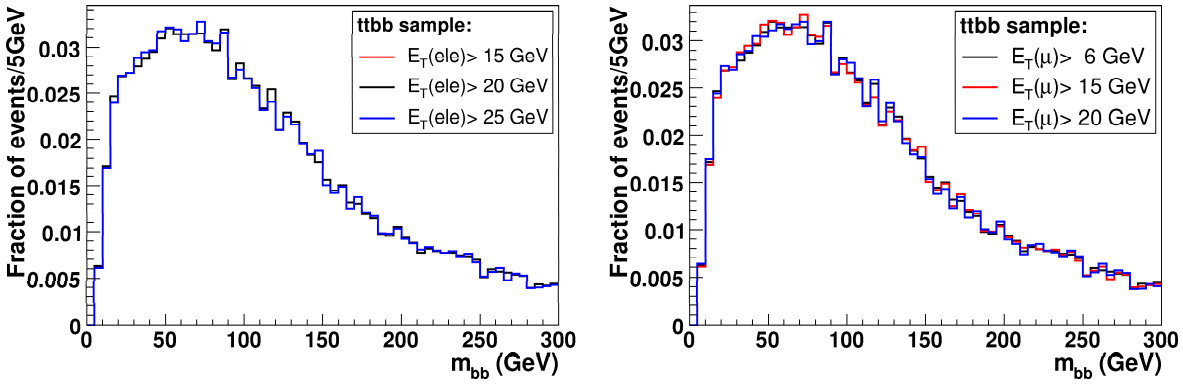

Figure 3.5: Mass spectrum $m_{b\bar{b}}$ of $t\bar{t}b\bar{b}$ sample with a cut variation of the transverse energy for electrons (right) and muons (left). All histograms are normalised to unit area.

sulting mass spectra $m_{b\bar{b}}$ are shown for the $t\bar{t}b\bar{b}$ sample in figure 3.5. For muons, cuts of 6GeV (standard selection cut), 15GeV and 20GeV were applied and for electrons, cuts of 15GeV, 20 GeV (standard selection cut), 25 GeV were applied. Since there is no significant change in the $m_{b\bar{b}}$ shape for those cuts, it can be concluded that the Higgs mass distribution is not that sensitive to the lepton p_T cuts. Due to recently increased trigger thresholds in ATLAS, it is intended to change these cuts in future to: $E_T(e) > 25GeV$ and $E_T(\mu) > 20GeV$.

The left plot in Figure 3.6 shows the mass spectrum of all reconstructed hadronic W boson candidates. Only those candidates in the mass window $m_W \pm 25GeV$ of the nominal W boson mass are considered for reconstruction of the top quark. A noticeable peak around the W boson mass is visible, but also a large combinatorial contribution where wrong combinations of light jets were chosen. The effects of tightening the mass window cut of $\pm 20GeV$ and $\pm 15GeV$ on the background shape in the $m_{b\bar{b}}$ mass spectrum can be seen in figure 3.6 (right). A significant change in the background shape is not visible. A reason for this could possibly be that only a small fraction of the relevant m_{jj} mass window is actually correctly combined jets and that by tightening this window, only more combinatorics will be considered.

As shown in the previous section, there are clearly more jets at lower p_T in background than observed in signal. Since in the jet preselection a general p_T is applied for both light and b-jets, a separate, higher cut on b-jets is considered. The p_T distribution for b-jets for signal and background events is compared in figure 3.7 (left). A cut on $p_T > 25GeV$ was applied. The effect on the background shape in the $m_{b\bar{b}}$ mass spectrum is shown in figure 3.7 (right). There is a noticeable change in the background shape where the peak of the distribution has been shifted to higher values of the $m_{b\bar{b}}$ spectrum.

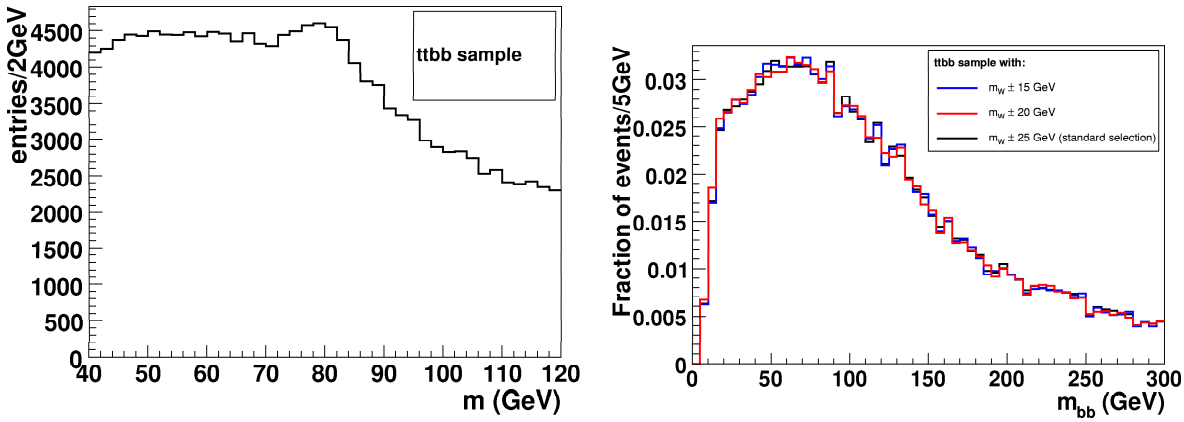

Figure 3.6: Left: Mass spectrum of all reconstructed hadronic W boson candidates. Right: m_{bb} mass spectrum of Higgs candidates with variation of W mass window cut, normalized to unit area.

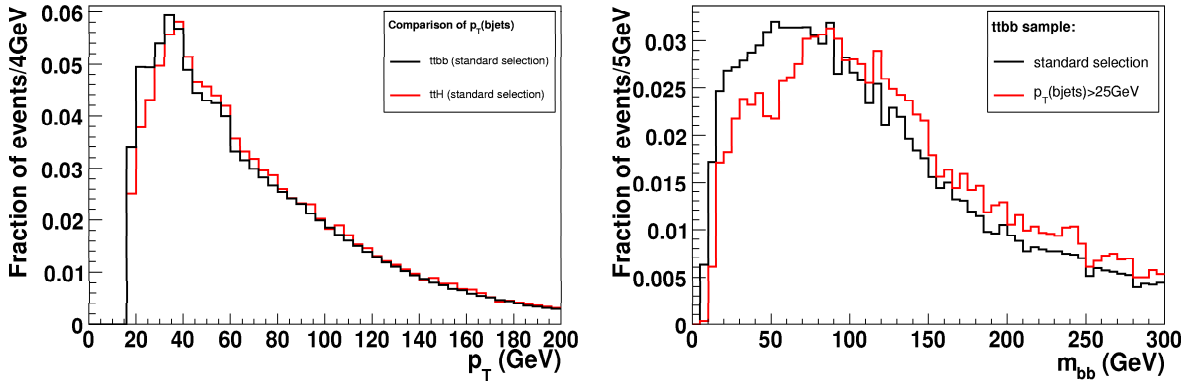

Figure 3.7: Right: p_T distribution for b-jets after the preselection. Left: Effect of applying a cut on p_T(b-jets) on shape in m_{bb} mass spectrum for $t\bar{t}b\bar{b}$ events. Both histograms are normalized to unit area.

This noticeable effect in the $t\bar{t}b\bar{b}$ background shape due to the b-jet p_T cut gives rise to the idea of considering a p_T cut on b-jets that are reconstructed as decay products of the Higgs boson. The Higgs reconstruction, the final step of the analysis, picks the best combination of the remaining b-jets, which weren't associated to the top decays. These are ordered in p_T and the Higgs candidate is reconstructed by combining the two b-jets with the highest p_T.The p_T distributions for the first and second highest b-jets in p_T are shown for signal and background

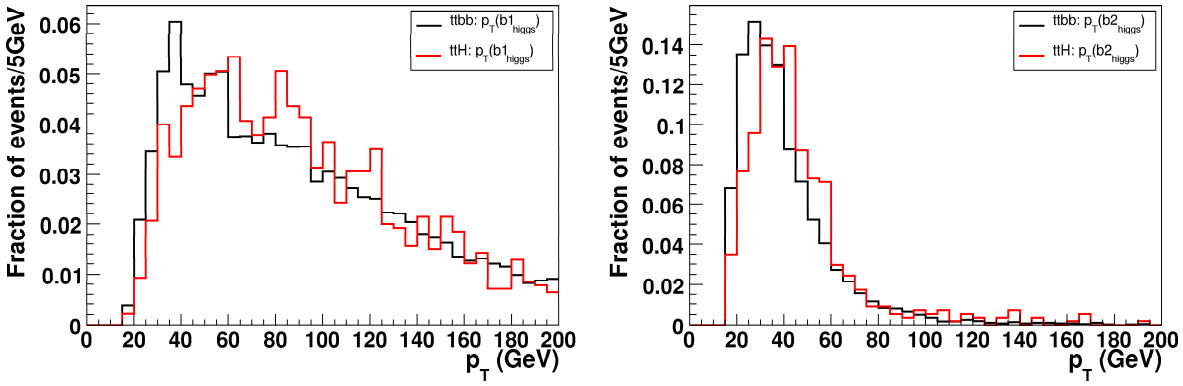

Figure 3.8: Comparison of p_T distribution of $t\bar{t}H^0$ and $t\bar{t}b\bar{b}$ sample for the first (left) and second (right) highest b-jet in p_T . Both histograms were normalized to unit area.

events in figure 3.8. The $t\bar{t}H^0$ sample a harder p_T distribution in the low p_T region for the first b-jet and a more subtle harder distribution for the second b-jet than the $t\bar{t}b\bar{b}$ sample.

In order to view possible correlations, the p_T distribution of the first b-jet is plotted against that of the second b-jet in Figure 3.9 for all events (left plot) as well as for the m_{bb} mass range of interest, $90\text{GeV} < m_{bb} < 150\text{GeV}$ (right) for the $t\bar{t}b\bar{b}$ and $t\bar{t}H^0$ sample. The red lines in the 2D histograms mark where the cuts are actually applied and also show that the cuts have actually an effect on the events in the region of the Higgs mass. Neither the $t\bar{t}b\bar{b}$ nor the $t\bar{t}H^0$ b-jets seem to have a distinct correlation. Therefore a cut on $p_T(b_1) > 40\text{GeV}$ and of $p_T(b_2) > 30\text{GeV}$ is applied.

The resulting background shape is shown in figure 3.10. There is a significant change of the background shape visible, the peak is shifted to higher values of the invariant mass spectrum. Due to the asymmetric cuts on p_T , a peak at around 30GeV is visible. This is outside the mass region of interest however.

To be able to validate that these two p_T cuts on the b-jets of the reconstructed Higgs candidate actually increase the fraction of correct bb combinations, further studies have to be undertaken in the near future. Also further variables will eventually be considered in oder to study their effects on the background shape.

For the purposes of this study, a background distribution with significant shape differences to that of the signal has already been found and the standard selection with the additional two asymmetric p_T cuts on the b-jets from the Higgs candidate is considered for now as the *tight selection.*

The combined distribution of the $t\bar{t}b\bar{b}$ background and signal from a Higgs boson of $m_H = 120\text{GeV}$ reconstructed with the standard selection is shown in Figure 3.11 (left) and with the tight se-

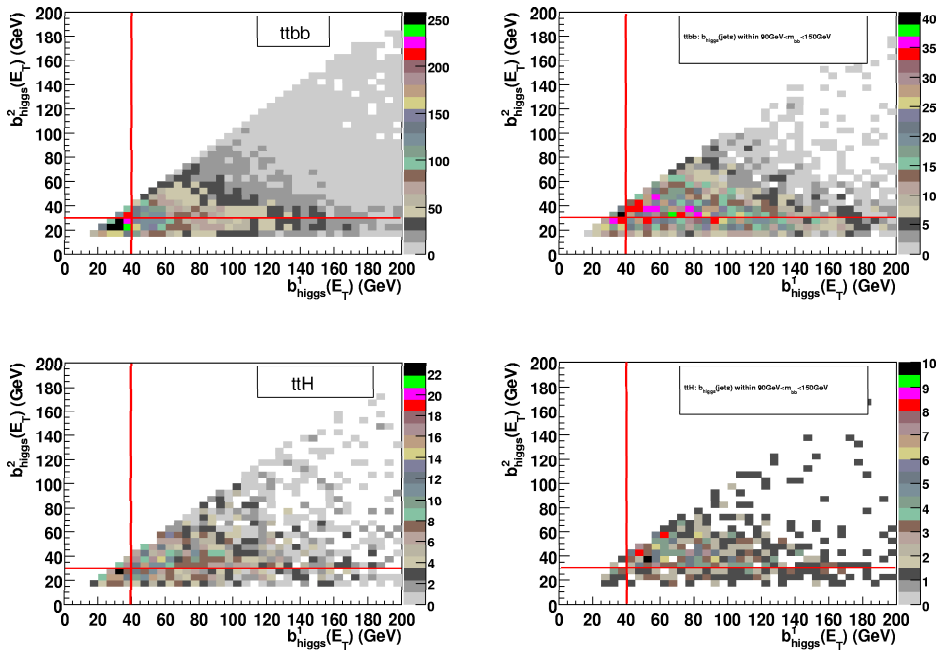

Figure 3.9: p_T distribution of the first b-jet plotted against second b-jet (left) and for the m_{bb} mass range of interest 90GeV $< m_{bb} <$ 150GeV (right) for $t\bar{t}b\bar{b}$ (top row) and $t\bar{t}H^0$ events (bottom row). The red lines mark the cuts which are applied.

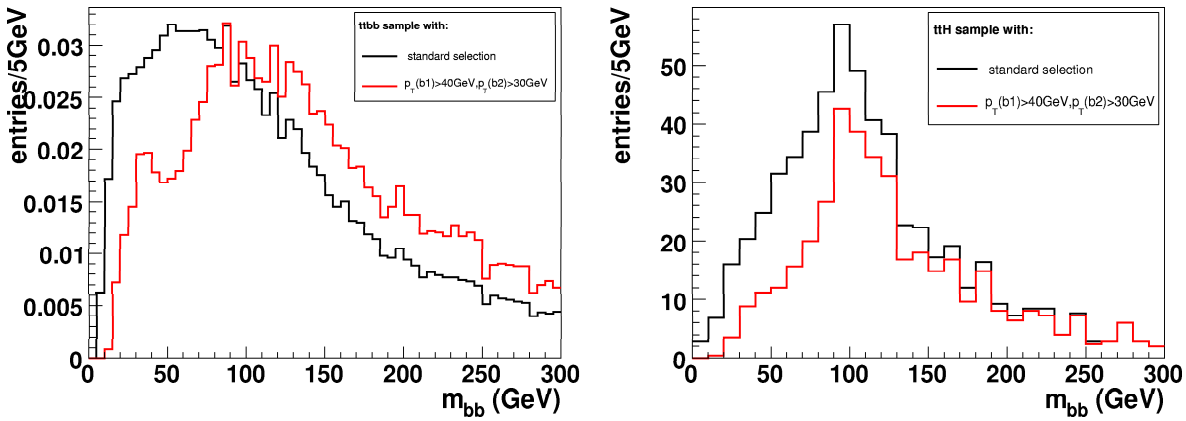

Figure 3.10: Left: Comparison of m_{bb} mass spectrum distribution for $t\bar{t}b\bar{b}$ events with and without the $p_T(b_1) > 40$GeV and $p_T(b_2) > 30$GeV cut. The histogram is normalized to unit area. Right:m_{bb} mass spectrum for signal events for standard (left) and tight selection (right), normalized to 30fb^{-1}.

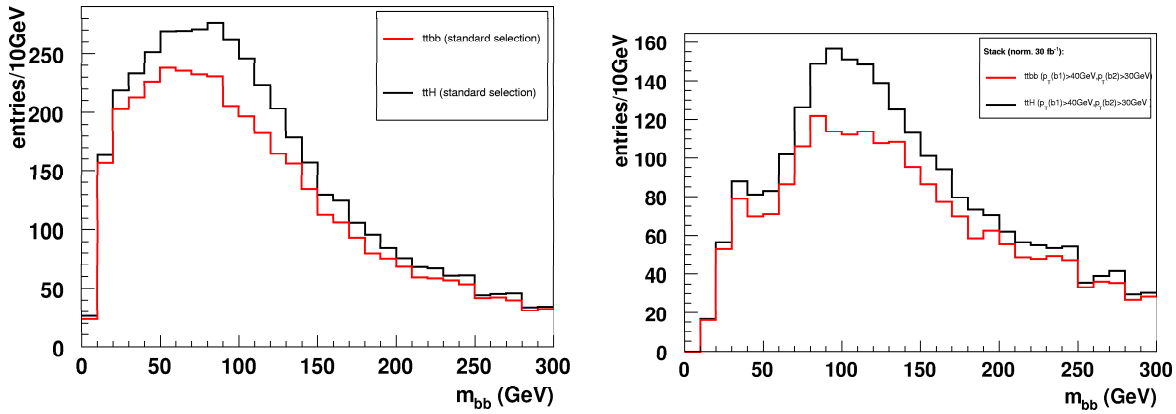

Figure 3.11: Combined reconstructed Higgs boson mass spectrum for $t\bar{t}b\bar{b}$ background and signal for standard (left) and tight selection (right), normalized to 30fb^{-1}.

lection in Figure 3.11 (right). Both distributions are normalized to expected event rates for an integrated luminosity of 30fb^{-1} (see Appendix C), which is equivalent to 3 years of initial LHC running. The distribution of signal events reconstructed with the tight selection appears to have a more distinctive peak (see also Figure 3.10 (right)) than the one from the standard selection. Therefore the combined shape of tight selected Higgs candidates is less similar to the $t\bar{t}b\bar{b}$ background shape than it is in the case for the standard selection. In both distribution, the m_{bb} spectrum shows a peak near the simulated Higgs boson mass for signal events with correctly identified b-jet pairings, but it reveals also large tails from events where the wrong b-jets are chosen. One thing to notice is that the peak appears at slightly lower masses than the generated mass. This can be more clearly seen in Figure 3.10 (right) which shows a comparison of the m_{bb} spectrum with standard and tight selection, normalized to unit area.

3.3.2 Fitting the background shape

A Landau distribution is fitted to both, the standard and tight selected $t\bar{t}b\bar{b}$ mass spectra:

$$\text{Landau} \quad = \quad c\frac{1}{x\sqrt{2\pi s^2}}e^{-(\ln x - m)^2/(2s^2)} \tag{3.3}$$

where m is the Most Probable Value and s the width of the distribution and c is a constant. The fit is applied in the mass range 50GeV $< m_{bb} <$ 300GeV and shown in Figure 3.12 for the standard (left) and tight selection (right). The resulting fit parameters for standard and tight selection are shown in table 3.2. The Landau distribution seems to show a reasonable fit, based on the χ^2 values.

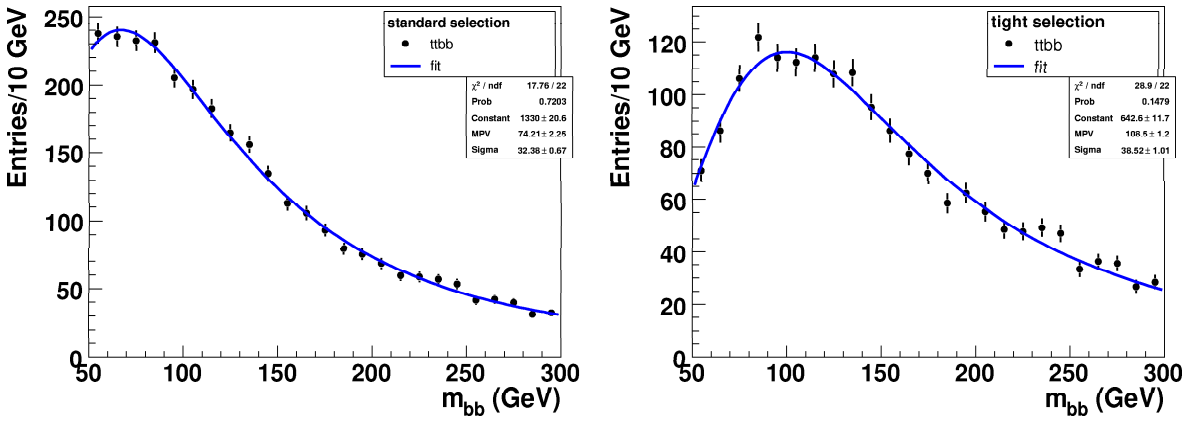

Figure 3.12: m_{bb} mass spectrum for $t\bar{t}b\bar{b}$ background events reconstructed with standard (left) and tight selection (right), normalized to 30fb^{-1}. The fitted Landau distribution is shown in blue.

selection	m	s	c	χ^2/n.d.f.
standard	74.21±2.25	32.38±0.67	1330±20.6	17.76/22
tight	108.5±1.2	38.52±1.01	642.6±11.7	28.9/22

Table 3.2: Fit parameters m_{bb} spectrum of standard and tight selected $t\bar{t}b\bar{b}$ events. A Landau distribution with the Most Probable Value m, the width of the distribution s and as well a normalization factor c. The resulting χ^2/n.d.f. and is also given.

3.3.3 Discussion of possible approaches for signal estimation

In order to be able to estimate the signal contribution in a combined distribution, two different approaches were undertaken and will be described in the following subsections.

Sideband fit

The $t\bar{t}b\bar{b}$ background and $t\bar{t}H^0$ sample are normalized to 30fb^{-1} to form a combined "data sample". Making the naive assumption that only background events and no signal events contribute to the sideband region of this sample (150GeV $< m_{bb} <$ 300GeV), a Landau distribution with fixed parameters of the Most Probable Value m and the width s of the distribution is fitted to this region in the m_{bb} mass spectrum. The values for m and s are obtained from the fit of the background over the whole range (section 3.3.2), only a scaling parameter is left free to vary. The result of this approach can be seen in Figure 3.13. With the fixed parameters and the scaling obtained from the fit, the Landau distribution is then drawn over the whole shown range. In

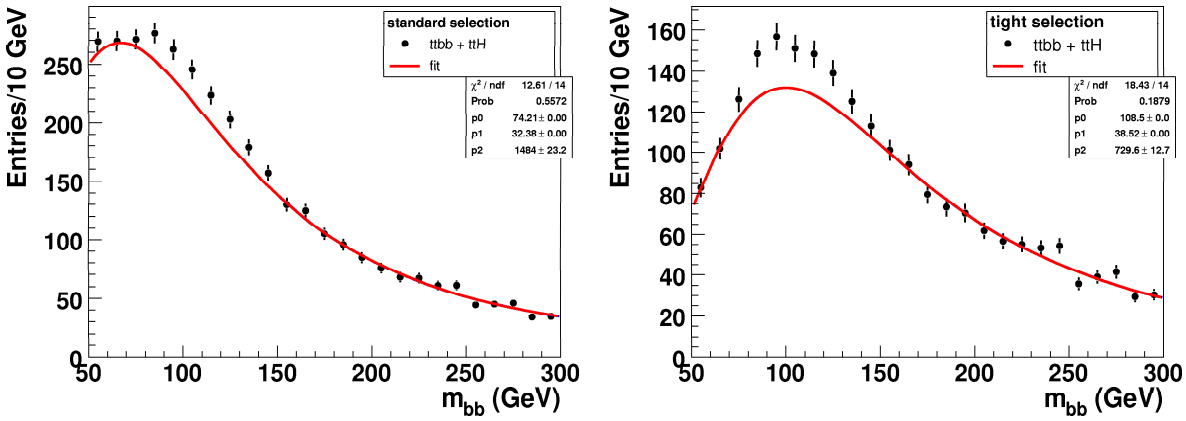

Figure 3.13: Combined m_{bb} mass spectrum for $t\bar{t}b\bar{b}$ background and signal for standard (left) and tight selection (right), normalized to 30fb^{-1}. A Landau distribution is fitted to the sideband 150GeV $< m_{bb} <$ 300GeV shape with most probable value and sigma fixed to values from fitting the background only (section 3.3.2).

selection	c	χ^2/n.d.f.	P(χ^2,n.d.f.)
standard	1482± 23.2	12.61/14	0.5572
tight	729.6±12.7	18.43/14	0.1879

Table 3.3: Scaling parameters obtained from the fit of the sideband region 150GeV $< m_{bb} <$ 300GeV for standard and tight selected events of the combined "data sample". The resulting χ^2/n.d.f. and probability and is also given.

table 3.3, the scaling parameters for the standard and tight selection as well as the χ^2/n.d.f and the Probability P(χ^2,n.d.f.) are shown. The χ^2 probability P(χ^2,n.d.f.) is a number between 0 and 1 that indicates how likely it is that for a given number of degrees of freedom, the χ^2 could be greater than the reported χ^2. A very small χ^2 probability indicates that it is unlikely that the measurements are all consistent with the expectation.
Comparing the probabilities for standard and tight selection, one can clearly see that with the developed tight selection, there is a greater visible discrepancy between the applied fit and the "data sample ". This shows that the application of the tighter selection improves the ability to statistically discriminate the signal.

From the assumption, that only background events are expected in the sideband region, it follows, that the signal contribution is in this approach underestimated. Therefore this approach is not optimal, but nevertheless shows, that it is a possibility of estimation signal events. In order to improve this technique, a sideband to higher values of m_{bb} could be chosen.

selection	c	χ^2/n.d.f.	P(χ^2,n.d.f.)
standard	1555± 13.7	41.89/24	0.01329
tight	770±8.6	54.12/24	0.0004105

Table 3.4: Scaling parameters obtained from the fit of the whole region of interest 50GeV < m_{bb} < 300GeV for standard and tight selected events of the combined "data sample". The resulting χ^2/n.d.f. and probability P(χ^2,n.d.f.) and is also given.

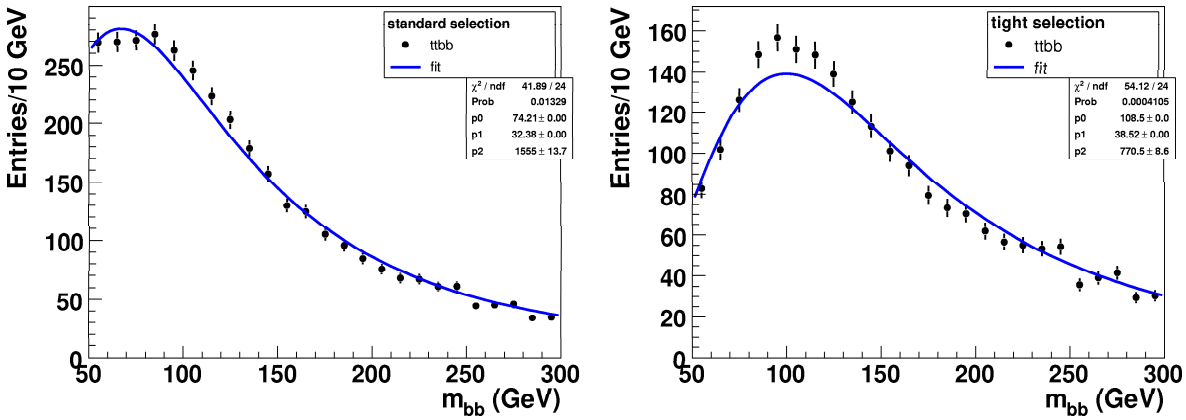

Figure 3.14: Combined reconstructed Higgs boson mass spectrum for $t\bar{t}b\bar{b}$ background and signal for standard (left) and tight selection (right), normalized to 30fb^{-1}. A Landau distribution is fitted to the shape with most probable value and sigma fixed to values from fitting the background only (section 3.3.2).

Combined fit

Since the sideband fit underestimates signal events, a different approach for signal estimation is applied.
Following the naive assumption that only background events contribute to the combined "data sample", a Landau distribution with the fixed values for the Most Probable value and the sigma from section 3.3.2 for both selections is fitted to the combined sample, but this time over the whole range of interest (50GeV< m_{bb} <300GeV). The scaling factor is the only free parameter. The results are shown in Figure 3.14, the obtained fit parameters are listed in table 3.4. The resulting fit and also the χ^2/n.d.f. and P(χ^2,n.d.f.) show that the chosen fit function does not describe the combined sample well. Again, there is a greater discrepancy between the applied fit and combined sample for the tight sample visible than for the standard selected sample.

In order to describe the additional $t\bar{t}H^0$ signal contribution, a description of the m_{bb} spectrum from signal events is necessary.

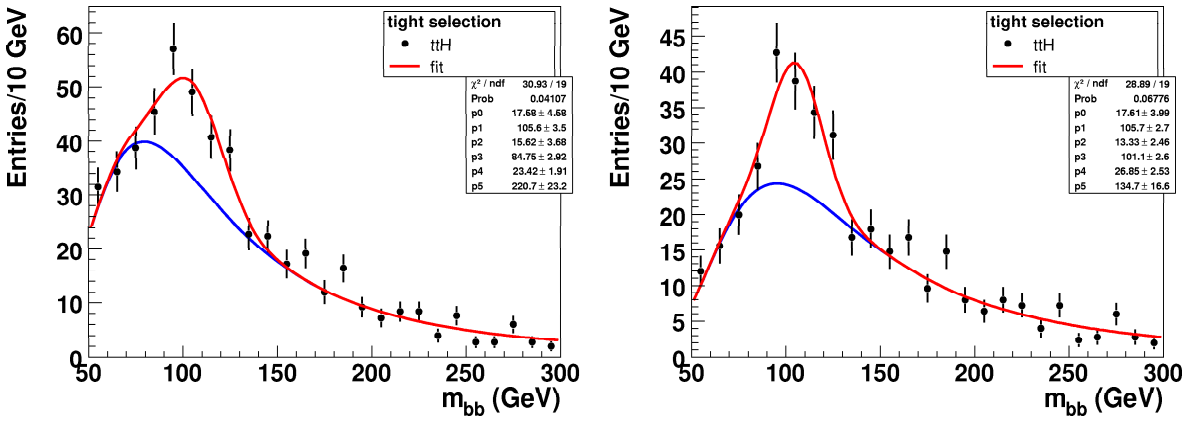

Figure 3.15: m_{bb} mass spectrum for $t\bar{t}H^0$ events. A Gaussian is fitted to the signal peak, a Landau distribution is fitted to account for the combinatorial part of incorrect combinations.

A Gaussian is fitted to the signal peak in order to determine the value and resolution of the reconstructed Higgs boson mass. This is accomplished by fitting a combination of a Landau distribution, to account for the combinatorial part:

$$\begin{aligned} \text{fit function } (t\bar{t}H^0 \text{ events}) &= \text{Gauss} + \text{Landau} \\ \text{Gauss} &= \frac{1}{\sigma\sqrt{2\pi}} e^{-(x-\mu)^2/(2\sigma)} \qquad (3.4) \\ \text{Landau} &= \frac{1}{x\sqrt{2\pi s^2}} e^{-(\ln x - m)^2/(2s^2)} \qquad (3.5) \end{aligned}$$

where μ is the mean and σ the standard derivation of the Gauss function are and m is the Most Probable Value and s the width of the Landau distribution are. The fit is applied in the mass range $50\text{GeV} < m_{bb} < 300\text{GeV}$. The left plot in Figure 3.15 shows the fit for the standard selection, the right plot shows the fit result for the tight selection. The resulting fit parameters for tight and standard selection are summarized in table 3.5.

Being aware of the inability to fit a pure signal sample in data, the fit function to the simulated signal events can nevertheless give an idea of how the signal contribution could be described, as well as possibly fix the fraction between correctly (which are described by a Gaussian distribution) and incorrectly (described by a Landau distribution) reconstructed Higgs candidates.

In order to fit the combined m_{bb} mass spectra, both the signal fit and the background fit are added to form a combined fit function:

$$\text{combined fit} = a \times \text{signal fit} + b \times \text{background fit} \qquad (3.6)$$

selection	μ	σ	n_{gauss}	m	s	n_{Landau}	χ^2/n.d.f.
standard	105.6±3.5	15.6±3.7	17.6±4.6	84.8±2.9	23.4±1.9	220.7±23.2	30.9/19
tight	105.7±2.7	13.3±2.5	17.6±3.9	101.1±2.6	26.9±2.5	134.7±16.6	28.9/19

Table 3.5: Resulting signal fit parameters for standard and tight selection using a Gaussian with mean μ, standard derivation σ and normalization n_{gauss} and a Landau distribution with the Most Probable Value m, the width of the distribution s and as well a normalization factor n_{Landau}. The resulting χ^2/n.d.f. is also given.

selection	a	b	χ^2/n.d.f.	P(χ^2,n.d.f.)
standard	0.9996±0.2087	1335±48	18.95/23	0.7039
tight	0.9867±0.1805	648.6±23.9	24.25/23	0.39

Table 3.6: Resulting fit parameters for standard and tight selection. a, b are the scaling parameters for the signal fit distribution and the background fit distribution. The resulting χ^2/n.d.f. is also given and probability P(χ^2,n.d.f.) is also given.

where a, b are the only free scaling parameters, all other parameters are fixed with the obtained values from the single fits. The obtained fit parameters are listed in table 3.6. In Figure 3.16 the fit for the combined m_{bb} spectra for standard and tight selection is shown.

In order to make a sensible evaluation of the goodness of the applied fits, the Kolmogorov-Smirnov test [8] is applied. The advantage of this test, compared to the χ^2 test, is that it is less sensitive to statistical fluctuations but more sensitive to differences in shapes between the compared distributions.
The Kolmogorov-Smirnov test tries to determine if the shape of two distributions differ significantly by returning a probability that they are statistically the same. Probabilities close to one imply very similar distributions, probabilities close to zero imply that the two distributions are substantially different. In table 3.7 the values from the Kolmogorov-Smirnov and χ^2 test are listed. Comparing the Kolmogorov probabilities among the standard and tight selection, it is obvious that the combined fits work much better than just the background fits. This is also confirmed by the χ^2 probability. Comparing the selections among the background and combined fit, it seems that for the tight selection there is a greater difference in the probabilities for both applied goodness of fit tests.

By comparing the goodness of the background and the combined fit it is possible to determine wether the considered sample is composed of purely background distributions or additionally of signal events.

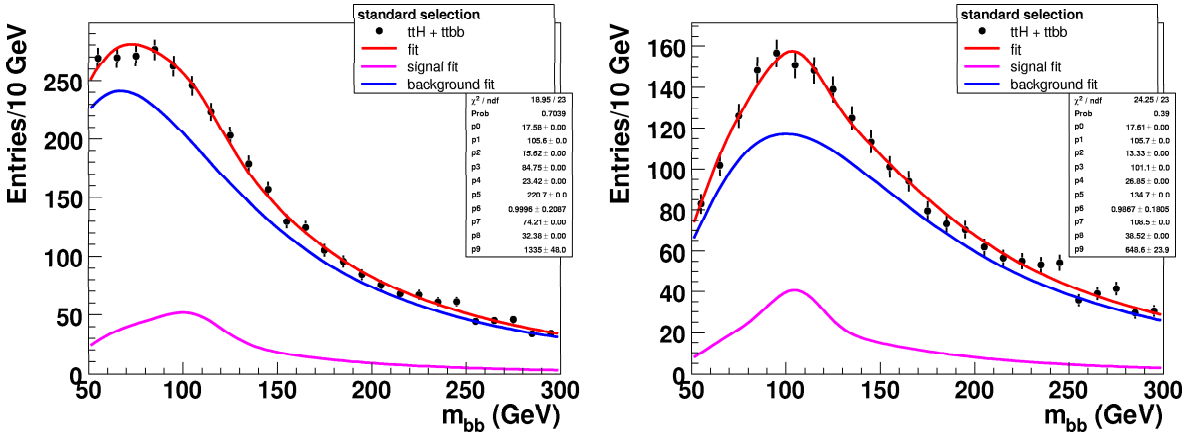

Figure 3.16: Combined reconstructed Higgs boson mass spectrum for $t\bar{t}b\bar{b}$ background and signal for standard (left) and tight selection (right), normalized to 30fb^{-1}.

selection	fit applied	D	$\sqrt{N}$	d (=D$\sqrt{N}$)	P(d)	P(χ^2,n.d.f.)
standard	background	0.0153	58.59	0.897	0.3972	0.0133
standard	combined	0.0040	58.59	0.235	1	0.7038
tight	background	0.0244	46.56	1.139	0.1487	0.0004
tight	combined	0.0072	46.56	0.335	0.9998	0.3899

Table 3.7: Summary of values of the Kolmogorov-Smirnov and χ^2 test. The listed parameters are explained in the text.

Summary and Future Plans

This report summarises the first eight month of the postgraduates studies. For an estimation and extraction of the $t\bar{t}H^0$ signal peak in the m_{bb} mass spectrum it is important to know and understand the shape of the background, especially the contribution of the irreducible $t\bar{t}b\bar{b}$ background from QCD. With the undertaken study of the $t\bar{t}b\bar{b}$ background shape, the developed techniques of the sideband and combined fit show their capability with respect to their application in data in order to estimate signal contributions.
A contribution was also made to the ATLAS distributed analysis model (see appendix D).

The future work includes:

- Improvement of the tight selection.
- Improvement and further development of the sideband and combined fit methods.
- Undertake a Toy Monte Carlo study as a further goodness of fit method.
- Consideration of all possible background contributions, such as e.g. ttjj.
- Test the developed fit methods with respect to sucessivly loosening the b-tagging.
- Study the badly reconstruced Higgs candidates in detail and comparison of shape with background events.

This will lead to a better understanding of the behaviour of all contributing backgrounds to the $t\bar{t}H^0$ channel and help to be able to estimate the signal contribution.
There is also the more technical work which is part of my PhD thesis, which will be to work on the Level 2 trigger.

A Event Generation and Simulation

Analysis in ATLAS are performed on generated Monte Carlo events, since the LHC is currently under construction. The generation of such Monte Carlo events is carried out in two main steps. An event generator is used to simulate the relevant physics processes with the same average behaviour and fluctuations as expected from real data. This is then followed by a simulation of the detector response. Finally the analysis code is used to run on those events in order to select the relevant signal events.

A.0.4 Event Generation

The objective of an event generator is to generate events as detailed as it could possible be observed by an perfect detector. There are two event generators being used in this report to generate the signal and background processes of interest.

Pythia [10] is a general purpose Monte Carlo generator for multiparticle production at e^+e^-, pp and ep colliders. Around three hundred different partonic processes at leading order are provided . The basic hard process is generated through the calculation of matrix elements. By adding initial and final state radiation and showers to the hard process, a more realistic description is obtained. Partons are hadronised using the Lund symmetric string fragmentation model [11]. Partons are connected via „strings „. As two partons move apart the potential energy stored in the string connecting them increases until it is possible for the string to break, producing a $q\bar{q}$ pair. The system now consists of two colour singlet $q\bar{q}$ pairs and, if the energy stored in their strings is large enough, further breaks will occur until only on-mass-shell hadrons remain.

AcerMC [7] is a dedicated event generator for Standard Model background processes in pp collisions at the LHC. The processes provided are characterised by heavy flavour jets and/or multiple isolated leptons in the final state. These processes have large matrix element expressions, therefore it is necessary to tailor the phase-space selection procedure to the dynamics of the process in order to achieve a reasonable generation efficiency. The program itself provides a library of the massive matrix elements and phase space modules for generation of a set of selected processes. The hard process events, generated with one of these modules, can be completed by the initial and final state radiation, hadronisation and decays, simulated with either PYTHIA 6.3, ARIADNE 4.1 or HERWIG 6.5 Monte-Carlo event generators. AcerMC includes the processes

$gg, q\bar{q} \rightarrow t\bar{t}b\bar{b}$ and $gg, q\bar{q} \rightarrow (Z/W/\gamma^* \rightarrow)t\bar{t}b\bar{b}$ which are important backgrounds for the Higgs production and decay channel that is the focus of this report.

A.0.5 Detector Simulation

The ATLAS experiment has two main simulations of the detector. These are the full and the fast simulation.
The full simulation is based on GEANT4 [12]. The full chain of detector simulation and event reconstruction is very time-consuming, especially for complex detectors as the ATLAS detector.
The fast simulation is called Atlfast [13] (ATLas FAST simulation package). It replaces the full detector simulation and reconstruction phases of the Monte Carlo reconstruction chain. Fast simulation is performed by smearing the MC truth information directly with resolutions measured in full simulation studies. Atlfast is a very practical tool for high-statistics studies, providing the most crucial aspects of the detector response: jet reconstruction in the calorimeters, momentum/energy smearing for leptons and photons, magnetic field effects and missing transverse energy.

B B-tagging

In full simulation a jet is tagged as a b-jet when the jet weight is greater than 3. The calculation of a weight for a jet is based on the impact parameter, the distance to the closest approach to the primary vertex. Hadrons containing b-quarks do have a non-zero distance due to their substantially larger lifetime.
The jet weight is calculated from the tack significance by calculating the significance S_i for each track i. The ratio of the values of the significance probability distribution functions for b-jets and u-jets is computed:

$$r_i = \frac{f_b(S_i)}{f_u(S_i)}. \tag{B.1}$$

Then the jet weight is constructed from the sum of the logarithms of the ratios:

$$W = \sum_i \log r_i. \tag{B.2}$$

This calculation is based on the impact parameter a_0, the non-zero distance to the closet approach to the primary vertex, from which the significance is gained. Figure B.1 shows the significance distribution for u- and b-quarks (left) and the jet weights from the likelihood ratio (right). These comparisons were made with decay samples $pp \rightarrow ZH/WH$ where $H \rightarrow b\bar{b}$ and $H \rightarrow u\bar{u}$ with $m_H = 100GeV$ [5].

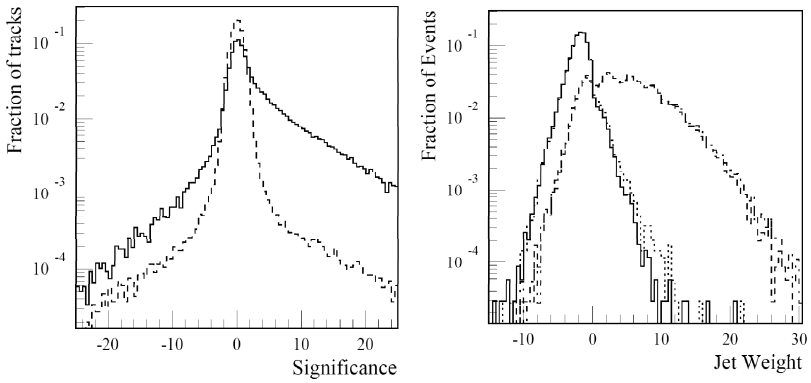

Figure B.1: Left: Significance Distribution: signed impact parameter divided by its error. Curves for b-jets (solid) and u-jets (dashed) are normalized to the same area. Right: Jet weights for b-jets (dashed line) and for u-jets (solid line) [5].

C Scaling to Luminosity

To get the expected number of events for the signal and the background processes for integrated luminosity L, the final histograms are scaled by a factor F of:

$$F = \frac{L_{wanted}\sigma_{gen}}{N_{gen}} \tag{C.1}$$

where N_{gen} is the number of generated events, L_{wanted} is the Luminosity to which the number of events are scaled to and σ_{gen} is the cross section of the process considered. In table C.1, the parameters and the resulting scaling value are listed.

process	σ_{gen}	N_{gen}	L_{wanted}	F
$t\bar{t}b\bar{b}$ (QCD)	0.519pb	1M	$30fb^{-1}$	0.24
$t\bar{t}H^0$	8.1pb	38950	$30fb^{-1}$	0.39

Table C.1: Efficiencies for the $t\bar{t}H^0$ signal and $t\bar{t}b\bar{b}$ background sample after the Lepton and Jet Preselection, the leptonic and hadronic W reconstruction, the $t\bar{t}$ and finally the Higgs boson reconstruction.

D The ATLAS Distributed Analysis model

The aim of the distributed analysis project is to enable individual ATLAS users to use Grid resources for their analysis in physics and detector groups. While currently it is not a trivial operation to submit jobs to the Grid, facilitating access to the Grid for analysis users has to been foreseen since the computing needs after the start of LHC will require the use of Grid resources in order to support analysis.
The strategy of the distributed analysis model exploits the existing grid infrastructure directly via the various supported grid flavours and also indirectly via the ATLAS Production System (Prodsys). A display of this strategy is shown in Figure D.1.

D.1 Frontend Clients

GANGA (Gaudi, Athena aNd Grid Alliance) is the frontend tool being used for job definition and management. It provides distributed analysis users with access to multiple backends (e.g. LCG, NorduGrid etc.). A job in GANGA is constructed from a set of building blocks. All jobs must specify the software to be run (application) and the processing system (backend) to be used. Many jobs will specify an input dataset to be read and/or an output dataset to be produced. Input datasets for processing an Athena job can be selected via the Atlas Metadata Interface (AMI), a bookkeeping tool for the ATLAS Monte Carlo production. Optionally, a

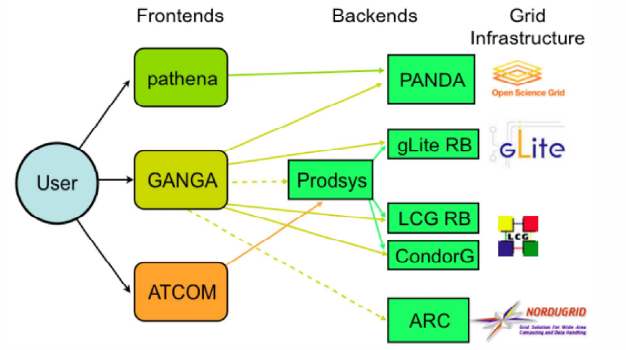

Figure D.1: Distributed analysis strategy [14].

job may also define functions (splitters and mergers) for dividing a job into subjobs that can be processed in parallel, and for combining the resultant outputs. GANGA is implemented in Python and currently provides two user interface clients: a Command Line Interface (CLI) and a Graphical User Interface (GUI).

D.2 Backends and Grid Infrastructure

Grids enable researchers to create a job, specify its requirements and submit it without worrying about selecting a valid computational site for executing their job. The Grid middleware takes care of monitoring the individual sites and choosing a valid location for user submitted jobs. Whether the job is successful or not depends on whether the application is able to start and complete its calculations on the remote site, and on whether the application output is returned to the user.

The LHC Computing Grid (LCG) [15] is by default the main ATLAS distributed analysis target system. Access to the LHC grid resources is possible via the LCG Resource Broker (RB). NorduGrid's [17] Advanced Resource Connector (ARC) is a second major production-ready Grid middleware solution. Even though the middleware technologies are based on same principle, there are substantial architectural and implementational divergences [18].

D.3 Personal experiences

The usage of grid facilities is of high importance, especially when the ATLAS detector is taking data. Therefore the aim was to run on the data samples available on the grid with the analysis code described in 3.1. The GANGA frontend tool was used in order to submit jobs to both, the LCG and NorduGrid. Before being able to successfully submit jobs and make them actually work on the different backends, several difficulties arose of which only a few will be mentioned here.

The ATLAS Computing model foresees only local access of data. This requires that the location of data has to be determined to send jobs to the corresponding sites. The ATLAS DDM groups files in datasets, provides information on the dataset location (Dataset Location Catalog) and the state of a dataset on a site which can be complete or incomplete). It was experienced with the LCG backend that it is notoriously difficult to guarantee the completeness of a dataset at a specific site. Using the automatic matching option to avoid specifying a computing element to submit an Athena job to will result most likely in a crash of the job because the job will most likely be sent to a site where the dataset is empty. This is related to the fact that the resource broker can't handle the concept of incomplete datasets. For incomplete datasets it can be anything from zero to all files of a dataset. On the LCG backend the best way is therefore

to find a site of a complete dataset. If datasets are not complete, one has to specify the name of a computing element to which the job will be sent.

Since GANGA version 4.3.0, it is also possible to submit jobs to NorduGrid. Using the NorduGrid backend, it was achieved to successfully run with the current analysis (12.0.6) on the complete $t\bar{t}b\bar{b}$ dataset. In collaboration with Adam Davison a TWiki page [20] with instructions on how to setup and use Ganga was made to summarize the work experience with Ganga and the LCG and NorduGrid.

Bibliography

[1] P. W. Higgs, Phys. Rev. Lett. 13 (1964) 508-509.

[2] M. Spira. QCD effects in Higgs physics. *Fortsch. Phys.*, 46:203-284, 1998

[3] ATLAS - Detector and Physics Performance, Technical Design Report, Volume 2, 25 May 1999, http://atlas.web.cern.ch/Atlas/GROUPS/PHYSICS/TDR/physics_tdr/printout/Volume_II.pdf.

[4] http://lhc.web.cern.ch/lhc/

[5] ATLAS - Detector and Physics Performance, Technical Design Report, Volume 1, 25 May 1999, http://atlas.web.cern.ch/Atlas/GROUPS/PHYSICS/TDR/physics_tdr/printout/Volume_I.pdf.

[6] ATLAS "High-Level Trigger Data Acquistion and Controls", Technical Design Report (CERN/LHCC/2003-022).

[7] http://borut.web.cern.ch/borut/

[8] W. T. Eadie *et al.*,*Statistical Methods in Experimental Physics*, 1971, 269-270.

[9] http://root.cern.ch/root/html/TMath.html

[10] http://www.thep.lu.se/ torbjorn/Pythia.html

[11] B. Anderson, *The lund model*, Camb. Monogr. Part. Phys. Nucl. Phys. Cosmol., 7:1-471, 1997.

[12] S. Agostinelli *et. all.*, *Geant4 - a simulation toolkit*, Nuclear Instruments and Methods in Physics Research, A 506 (2003) 250-303.

[13] E. Richter-Was and D. Froidevaus, *Atlfast 2.0 a fast simulation package for ATLAS*, November 1998, ATLAS Internal Note.

[14] K. Harrison, R.W.L. Jones, D. Liko, C.L. Tan, *Distributed Analysis in the ATLAS experiment*

[15] http://lcg.web.cern.ch/LCG/

[16] http://www.cs.wisc.edu/condor/condorg

[17] The NorduGrid Collaboration. [Online]. Available: http://www.nordugrid.org

[18] M.Gronager et al., *LCG and ARC middleware interoperability*

[19] http://lpsc1168x.in2p3.fr:8080/opencms/opencms/AMI/www/index.html

[20] https://www.hep.ucl.ac.uk/twiki/bin/view/Main/AtlasGanga